Proceedings of the Combustion Institute 34 (2013) 1973–1980
S. Maeda, S. Sumiya, J. Kasahara, A. Matsuo

1. Title:

Initiation and Sustaining Mechanisms of Stabilized Oblique Detonation Waves around Projectiles

2. Authors and affiliations:

SHINICHI MAEDA[1], SATOSHI SUMIYA[1], JIRO KASAHARA[1] AND AKIKO MATSUO[2]

[1]*Department of Engineering Mechanics and Energy,*
University of Tsukuba,
1-1-1 Tennodai, Tsukuba, 305-8573, Japan
[2]*Department of Mechanical Engineering,*
Keio University,
3-14-1 Hiyoshi,Kohoku-ku, Yokohama, 223-8522, Japan

3. Corresponding author's complete contact information:

Mailing address:
Jiro KASAHARA, Department of Engineering Mechanics and Energy
University of Tsukuba, 3F bldg. room 109, 1-1-1 Tennodai, Tsukuba, 305-8573, Japan
Fax: +81-29-853-5267
Email: kasahara@kz.tsukuba.ac.jp

4. Colloquium that describes the research topic:

DETONATIONS, EXPLOSIONS and SUPERSONIC COMBUSTION including pulse-detonation and scramjet engines.

5. Total length of paper and method of determination:

6186 words (Method 1)

6. List word equivalent lengths for main text, nomenclature, references, each figure with caption, and each table:

Main text: 3463 words
References: 437 words
Each table:
Table 1.: 228 words
Each figure:
Fig. 1.: 363 words, Fig. 2.: 112 words, Fig. 3.: 167 words, Fig. 4.: 170 words, Fig. 5.: 250 words,
Fig. 6.: 192 words, Fig. 7.: 418 words, Fig. 8.: 213 words, Fig. 9.: 173 words.

Abstract

Direct initiations and stabilizations of three-dimensional conical detonation waves were attained by launching spheres with 1.06 to 1.31 times the C-J velocities into detonable mixtures. We conducted high time-resolution Schlieren visualizations of the whole processes over unsteady initiations to stable propagations of the stabilized Oblique Detonation Waves (ODWs) using a high-speed camera. The detonable mixtures were stoichiometric oxygen mixtures with acetylene, ethylene or hydrogen. They were diluted with argon in a 50% volumetric fraction, and a 75% diluted mixture was also tested for the acetylene/oxygen. The direct initiation of detonation by the projectile and the DDT process like the Re-initiation appeared in the initiation process of stabilized ODW. This process eventually led to the stabilized ODW supported by the projectile velocity and the ringed shape detonation wave originating in the Re-initiation. We modeled the spatial evolution of stabilized ODW after the Re-initiation based on its C-J velocity and angle. The model qualitatively reproduced the measured development rate of stabilized ODW. We also discussed about the detonation stability for the curvature effect arising from the three-dimensional nature of stabilized ODW around the projectile. The curvature effect attenuated the detonation wave below its C-J velocity at the vicinity of projectile. The propagation limits of curvature effect will be responsible for the criticality to attain the stabilized ODWs. By accessing the detailed distributions of propagation velocities and curvature radiuses, the critical curvature radiuses normalized by the cell sizes experimentally revealed to be 8 to 10 or 15 to 18 for mixtures diluted with each 50% argon or 75% argon / krypton.

(258 words)

Keywords

Hypersonic Projectiles, Oblique Detonation Waves, Detonation Initiation, High-speed Camera

1. Introduction

Detonation initiations and stabilizations by projectiles [1, 2] have been conducted as fundamental studies of combustion processes in a ram-accelerator [3] and an oblique detonation wave (ODW) engine [4]. Lee [5] and Vasiljev [6] evaluated the critical energy for detonation initiation using the hypersonic blast wave analogy. Higgins and Bruckner [7] experimentally confirmed the initiation criticality if the projectile velocities were below to slightly above the Chapman-Jouget (C-J) velocity of the detonable mixture. Kasahara et al. [8] extended the projectile velocities through approx. 1.8 times the C-J velocity. They concluded that the criticality to stabilize a detonation wave, i.e., the stabilized ODW, was almost constant against the projectile velocities. This indicates that the proper local conditions (such as the curvature radius of the detonation wave) are also required for the stabilization, in addition to the energetic condition for the initiation, which becomes easy as the projectile velocity is increased.

Several previous studies [9-12] investigated such local conditions by calculating the distributions of the induction times or lengths behind a shock wave around a projectile. For the conditions slightly below the stabilization criticality, some visualization studies showed the possibilities of unsteady propagation regimes [8, 9, 13] in which the Deflagration to Detonation Transition (DDT) occurred behind the bow shock around the sphere projectile. Our previous studies [14, 15] revealed the propagation mechanisms and wave structures of unsteady regimes via high time-resolution Schlieren visualizations using a high-speed camera. Although these unsteady regimes were dominated by the complex and unstable DDT process, the stabilized ODWs were dominated by the continuous direct initiation of the overdriven detonation by the projectile and the attenuation of it by the expansion

waves [13]. The stabilized ODWs are inherently three-dimensional conical geometries, and have finite curvature radiuses. Our previous studies [15, 16] showed that the detonation wave near the projectile was attenuated below the C-J velocity by the curvature effect.

In the present study, we directly visualized detailed temporal evolutions of the whole process from initiation to stabilization of the ODW around the projectile. The first focus of our investigation was the unsteady initiation process just after the projectile fires the detonable mixture. Although previous studies have observed ODWs in the vicinity of projectiles, the present study revealed that the ODWs were followed by ringed detonation waves originating the unsteady initiation process far away from the projectiles. To our knowledge, such visualizations of the initiation processes have been obtained only in this study to date. We also investigated whether the diaphragm rupture by the projectile at the chamber inlet affects the stabilization criticality, as Higgins and Bruckner [7] pointed out for the initiation criticality. The second focus of our investigation was what local conditions dominate the criticality to stabilize the ODW around the projectile. We proposed that the curvature effect dominates the stabilization criticality, and we experimentally investigated the critical curvature radiuses in various mixture compositions by accessing the detailed distributions of propagation velocity and curvature radius. The curved detonation waves propagate not only around the projectiles but also inside the rotating detonation engines (RDEs), and therefore further studies of curvature effects in gaseous detonations will be needed to gain fundamental knowledge for applications of detonation waves.

(531 words)

2. Experimental Setup and Conditions

The experimental setup was nearly identical to that used in our previous studies [8, 14-16], therefore, only the essentials are given here. The two-stage light-gas gun launched the projectile with velocities 2000m/s to 2500m/s into the detonable mixture. The observation chamber that filled with the detonable mixture had glass windows for optical access. A Schlieren system and high-speed camera (HPV-1, Shimadzu) visualized the flowfields. The visualized region was circular with a 90-mm dia., and the center of this region was located 400 mm downstream of a Mylar diaphragm (12-μm thickness) dividing the detonable mixture from the gas gun. The high-speed camera recorded with a 1-μs frame speed, 250-ns exposure time, 312 × 260 spatial resolutions, and 100 continuous frames. The projectile was a sphere made of polyethylene, with a 4.76-mm dia.. The diameter of the observation chamber was considerably larger (approx. 63 times that of the projectile) to avoid the influence of wall reflections on the phenomena.

The experimental conditions are listed in Table 1. The detonable mixtures were stoichiometric oxygen mixtures with acetylene, ethylene or hydrogen. Each mixture was diluted with argon in a 50% volumetric fraction to make the C-J velocity lower than the projectile velocity. For the acetylene/oxygen mixture, a 75% dilution was also tested. The projectile velocities and detonabilities of the mixtures are expressed by the nondimensional projectile velocity (V_p / D_{CJ}, V_p: projectile velocity, D_{CJ}: C-J velocity) and nondimensional projectile diameter (d / λ, d: projectile diameter, λ: cell size) as used in previous studies [5, 7, 8, 14-16]. The detonabilities were controlled by varying the filling pressures, and are represented by the cell sizes accessed from the Detonation Database [17]. For each mixture, fitting equations for cell sizes as an exponential of filling pressures were used to interpolate or

extrapolate for each condition. The C-J velocities were calculated by STANJAN [18]. The projectile velocities were determined using dozens of continuous pictures from the high-speed camera. The projectile locations were situated almost linearly over time, and thus velocity deficits in the visualized region were negligible.

For visualizing the initiation process of stabilized ODWs, we attached flanges to set a diaphragm inside the visualized region. These tests were conducted using only a $2C_2H_2+5O_2+7Ar$ mixture. Two inlet conditions (w/ and w/o diaphragm rapture, in Table 1) were used to directly investigate whether the diaphragm rapture effect affected the generation of the stabilized ODW. In the w/ diaphragm rapture case, the projectile initially flew into a vacuumed section and broke the Mylar diaphragm (which had the same thickness as the chamber inlet) before firing the detonable mixture. In the w/o diaphragm rapture case, the projectile flew though a 15-mm-dia. hole opened at the center of the Mylar diaphragm (100-μm thickness). The detonable mixture was filled in both sides of the diaphragm, and the stabilized ODW around the projectile was quenched once at the passage across the hole.

(484 words)

3. Results and Discussion

3.1. Initiation Process of the Stabilized ODW

Figure 1 shows continuous pictures of the initiation process of stabilized ODW in the two cases, w/ and w/o diaphragm rapture, observed in almost the same V_p / D_{CJ} and d / λ. In the w/o diaphragm rapture case, the flowfields around the projectile were asymmetrical against the projectile axis, because of the offset between the center of the projectile and the hole in the diaphragm. In the w/ diaphragm rapture case, many diaphragm fragments flew around the projectile just after the diaphragm rapture. The projectile initially initiated a stabilized ODW just around it; however, away from the projectile, the ODW was diffracted and eventually separated the shock from the combustion wave (right pictures). The stabilized ODW developed over time, and the projectile continuously initiated a new detonation front. When the curvature radiuses of diffracted detonation and shock waves had grown sufficiently, the DDT process (like a re-initiation) initiated a new detonation wave (middle pictures). Such a re-initiation around the projectile was observed by Kasahara et al. [13]. This generated an almost toroidally expanding C-J detonation wave. Finally, these two ignition sources (the projectile and re-initiation) led to a stabilized ODW supported by the projectile velocity and a ringed detonation wave originating the re-initiation (left pictures). Regardless of whether the scenarios was w/ or w/o diaphragm rapture, similar temporal evolutions were observed above d / λ = 3.0-3.5. This criticality agreed with that found in our previous studies [14, 15] to attain the stabilized ODW using the same mixture. Below this criticality, the direct initiation ahead of the projectile failed, and the bow shock and shock-induced combustion were observed.

Figure 2 is a schematic of the temporal evolution of the observed initiation process. A cylindrical coordinate

was applied such that the *z* and *r* axes adapt to the flight direction of the projectile and a direction perpendicular to it. If the projectile can directly initiate the detonation wave on its nose, such as with a blunt-nose or cone-nose with a large half-angle, a qualitatively similar initiation process will be observed independent of the projectile shapes and sizes. In addition, as long as the ringed detonation wave remains self-sustained propagation and does not reflect with the chamber wall, the stabilized ODW followed by the ringed detonation will be maintained.

By using several assumptions, we modeled the *r*-direction evolution of the stabilized ODW after the re-initiation. The re-initiation occurred at the time t_{re} and location r_{re} as shown in Fig. 2. At arbitrary time *t* after the re-initiation, r_{ODW} denotes the outer edge location of the stabilized ODW. We assume that $r_{ODW} = r_{re}$ at time t_{re}, and the ringed detonation wave instantaneously starts to propagate from r_{re} with spatially uniform curvature radiuses. We also assumed that the stabilized ODW developed as a tangential line of a ringed detonation wave. The geometric relation in the right triangle ABC in Fig. 2 is:

$$\left(r_{ODW} - r_{re}\right) \Big/ \left\{ D_{CJ}\left(t - t_{re}\right) \right\} = \sin(90^\circ - \beta_{CJ}) . \quad (1)$$

Here, β_{CJ} denotes the wave angle of stabilized ODW (C-J angle), and is expressed as $\beta_{CJ} = \sin^{-1}(D_{CJ} / V_p)$. Therefore, the temporal evolution of r_{ODW} can be written as:

$$r_{ODW} = r_{re} + D_{CJ}(t - t_{re}) \cos \beta_{CJ} . \quad (2)$$

Differentiating Eq. (2) about time leads to the development rate of r_{ODW} as:

$$\mathrm{d}r_{ODW} / \mathrm{d}t = D_{CJ} \cos \beta_{CJ} . \quad (3)$$

In Eq. (2), there are empirical values, t_{re} and r_{re}; however, there is no empirical value in Eq. (3).

From the continuous pictures, we measured the time histories of r_{ODW} as the conjunction between the stabilized

ODW appearing as a straight line inclining with the C-J angle and the ringed detonation wave. Figure 3 shows the comparisons of calculated and measured dr_{ODW} / dt values. The solid and dashed lines in the figure represent the calculated results using the maximum and minimum C-J velocity in the experimental conditions, but these were almost the same line. If the d / λ values were well above the criticality, the measured and theoretical results had similar trends. However, just above the criticality, the measured results had values smaller than the theoretical results. The modeling was made using the assumption that the propagation velocity of the ringed detonation wave was the constant C-J velocity of a plane detonation wave over time. When the time or r_{ODW} after the re-initiation was small, the curvature effect on the ringed detonation wave would not be negligible, and therefore, the equations were valid well after the re-initiation when the curvature effect became negligibly small. In the experimental results obtained just above the criticality, this assumption would not be satisfied in the time and spatial scales of visualizations, because the generation of the ringed detonation needed larger time and spatial scales than the results obtained well above the criticality.

(780 words)

3.2. Curvature Effect on the Detonation Wave Stabilized by the Projectile

Here we discuss the results obtained well downstream of the initiation process described in the previous section. For each mixture, the minimum d / λ values shown in Table 1 were fairly close to the criticality to attain the stabilized ODW. When the d / λ value decreased by about 0.5 (3.5–5.0kPa for the filling pressure) in these conditions, we observed unsteady regimes [14–16] characterized by the DDT behind the bow shock to initiate and sustain the ODW. Figure 4 shows the visualization results (upper half sides of the projectiles) of near (Fig. 4a.) and well above (Fig. 4b.) the criticality in the $2C_2H_2$+$5O_2$+21Ar mixture. We extracted the wave shapes from Fig. 4 and plotted them (Fig. 5) so as to set the origin on the projectile center. In both cases, the wave angles, β_w, well apart from the projectile almost coincided with the C-J angles, β_{CJ}. Near the criticality, the smaller β_w compared to the β_{CJ} was evident near the projectile, and leading to the concave wave shape. This indicates that the curvature effect attenuated the detonation wave below the C-J velocity where the curvature radius was small [16]. In the present study, we obtained detailed assessments regarding the distributions of wave curvature radiuses and propagation velocities.

We applied the following fitting function to the measured wave shapes as the function of x and y in Fig. 5:

$$x = -R - \Delta + R_c \cot^2 \beta_{asy} \left[\left\{ 1 + \left(y^2 \tan^2 \beta_{asy} \right) \Big/ \left(R_c^2 \right) \right\}^{1/2} - 1 \right] + m_1 \left\{ 1 - \exp\left(m_2 y \right) \right\}^{m_3} \quad (4)$$

The equation above (except for the last term on the right side) is the empirical equation used to estimate the bow-shock shape around a sphere-nosed or cone-nosed projectile flying in air with supersonic to hypersonic velocity as suggested by Billig [19]. The projectile radius R is determined as the experimental condition. Billig gave the empirical correlation about the shock stand-off distance Δ and wave curvature radius R_c at the vertex as

the function of flight Mach numbers. The β_{asy} denotes the asymptotic wave angle at infinity and coincides with the Mach angle in projectiles with no aft-body, such as spheres. In Fig. 5, the calculated bow shock shape is compared with the measured shape obtained by launching the sphere into the argon gas with Mach number 7.62. The shapes agreed very well. We added the last term on the right side in Eq. (4) to express the wave shape of stabilized ODW. However, the added term has no physical meaning. The role of this additional term was only to reproduce the wave shape by applying some fitting parameters, although this might also be possible by some other non-physical method. This method is creative in the sense that we could calculate in detail the whole distributions of propagation velocity and curvature radius by adding this term. We used the measured values for Δ and R_c, and the C-J angle for β_{asy}. The m_1, m_2 and m_3 in the added term were determined by fitting Eq. (4) to the measured wave shape using a least squares method. The fitted results well reproduced the wave shapes as shown in Fig. 5. From Eq. (4), we can calculate the first and second derivatives (dy / dx and d^2y / dx^2), and we can obtain the whole distribution of wave angle and curvature radius. Figure 6 provides definitions of the curvature radiuses and schematics of their distributions. We defined two components of curvature radiuses (R_1 and R_2). The R_1 arises from the axisymmetric wave shape and exists at the plane perpendicular to the space shown in Fig. 6. The R_1 always has positive values, and makes monotonic increases along the y direction. The R_2 exists at the space in Fig. 6. The R_2 has positive or negative values depending on the convex or concave wave shape, and becomes infinity in the straight wave. The curvature radius ρ of them has the geometric relation: $1 / \rho = 1 / R_1 + 1 / R_2$.

In Fig. 6, region 1 is the bow wave coming from the decay process of overdriven detonation initiated by the projectile, and region 3 is the self-sustained detonation coming from the acceleration process to the C-J velocity.

The positive values of the R_2 lead to $\rho < R_1$ in the bow wave, and the negative values of the R_2 lead to $\rho > R_1$ in the self-sustained detonation. Point 2 is the inflection point where the wave changes from convex to concave shape. This point is the characteristic point where the propagation velocities have the local minimum value below the C-J velocity and $\rho = R_1$ ($R_2 = \infty$). The curvature effect on the detonation wave (i.e., the so-called D_n-κ relation) will explain the occurrence of this point. Theoretical and computational analyses of the D_n-κ relation were given by He and Clavin [20] and Yao and Stewart [21]. Attenuations of the propagation velocity by the curvature effect are subject to the ratio of the curvature radius to the induction zone length inside the ZND structure, and the detonation wave cannot make the self-sustained propagation below some critical curvature radius. Nakayama et al. [22] concluded that the cell sizes dominated the D_n-κ relations in the multi-headed detonations in their experimental investigations using ethylene-oxygen mixtures.

Figure 7 shows the concept of criticality to stabilize the ODWs around the projectiles based on the propagation limit from the curvature effect. Figure 7a gives the schematics of the regimes. The “super-critical condition” is well above the criticality as shown in Fig. 4b. The “sub-critical condition” is the case in which the projectile cannot initiate the detonation wave and the bow shock and shock-induced combustion are observed. In addition, the “critical condition” is near the criticality, as shown in Fig. 4a. Starting from the point next to the vertex of the bow wave, we move the point along the direction of wave propagation over time. If we continuously measure the propagation velocity D_n and curvature radius ρ at the moving points, we can trace their distributions from the bow wave near the projectile to the ODW away from it, shown as a - b - c, a’- b’ – c’ or a” – b” – c” for each condition in Fig. 7. The bow wave, self-sustained detonation and local minimum point of propagation velocity are described

in the schematic of critical condition. Figure 7b schematically shows these temporal evolutions of the D_n and ρ normalized by the C-J velocities D_{CJ} and cell sizes λ of the planar detonation. This figure also shows relationship between D_n / D_{CJ} and ρ / λ of the curved self-sustained detonation known as the C-shaped curve. The criticality appears to that the temporal evolution of D_n / D_{CJ} and ρ / λ around the projectile meets the propagation limit of the curvature effect (path a” - b” - c”). Therefore, in the critical condition, the ρ / λ at the local minimum point of propagation velocity will represent the critical curvature radius of curved self-sustained detonation.

Figure 8 shows the measured and fitted results of D_n / D_{CJ} and R_1 / λ or ρ / λ in the two cases illustrated in Fig. 4. The error bars result from the spatial resolutions of picture. The local minimum point of propagation velocity is evident in the result of No. 2-4 (near the criticality). Except for the experimental results in Fig. 8, we could not find a way to determine the D_n-κ relation expressed by the mixture’s cell sizes, because the analyses of the D_n-κ relation based on the ZND structure [20, 21] could not quantitatively reproduce the experimental results dominated by the cellular structure. In Fig.8, self-propagating detonation wave in the result near the criticality shows the D_n-κ relation obtained experimentally. Figure 9 shows the measured ρ / λ (= R_1 / λ) at the local minimum point of propagation velocity (with an asterisk) against the filling pressures of each mixture. As seen in the figure, the critical curvature radiuses normalized by the cell sizes were below 8 to 10 or 15 to 18 for each dilution ratio. These minimum ρ^* / λ values were obtained near the criticality, and the local minimum values of propagation velocity were about 0.8 times the C-J velocity. Therefore, these values will be close to the propagation limits of curved self-sustained detonation. This means that the curvature limits normalized by the cell size will also depend on the regularity of cellular structure, like the critical tube diameter for the re-initiation [23].

Turbulent flow natures inside irregular cellular structures may contribute more to sustaining the transverse shock waves compared to regular structures.

(1421 words)

Conclusions

We visualized the unsteady initiation processes and following stable propagations of stabilized ODWs by high-time resolution Schlieren imaging, and we made the following conclusions.

The direct initiation of detonation by the projectile and DDT process, like the re-initiation, appeared in the initiation process of stabilized ODW. This process eventually led to the stabilized ODW supported by the projectile velocity and the ringed detonation wave originating in the re-initiation. We modeled the spatial evolution of stabilized ODW after the re-initiation based on its C-J velocity and angle. In addition, the model qualitatively reproduced the measured development rate of stabilized ODW.

We discussed the detonation stability for the curvature effect arising from the three-dimensional nature of stabilized ODW around the projectile. The curvature effect attenuated the detonation wave below its C-J velocity in the vicinity of the projectile. The propagation limit of the curvature effect will be responsible for the criticality to attain the stabilized ODW. By obtaining detailed distributions of propagation velocities and curvature radiuses, we found that the critical curvature radiuses normalized by the cell sizes were 8 to 10 and 15 to 18 for mixtures diluted with 50% argon and 75% argon / krypton, respectively.

(197 words)

Acknowledgements

This work was subsidized by the Ministry of Education, Culture, Sports, Science and Technology via a Grant-in-Aid for Scientific Research (A), No. 20241040; a Grant-in-Aid for Scientific Research (B), No. 21360411; and the Research Grant Program from the Institute of Space and Astronautical Science, the Japan Aerospace Exploration Agency.

(50 words)

References

[1] H.F. Lehr, Astronautica Acta 17 (1972) 589-597.

[2] S.Yu. Chernyavskii, N.N. Baulin, A.S. Mkrtumov, Combustion, Explosion, and Shock Waves 9 (1973) 687-690.

[3] A. Hertzberg, A.P. Bruckner, D.W. Bogdanoff, AIAA J. 26 (2) (1988) 195-203.

[4] J.M. Powers, Combustion in High-Speed Flows, Kluwer Academic Publishers, Boston, 1994, p.345-371.

[5] J.H.S. Lee, Prog. Astronaut. Aeronaut. 173 (1997) 293-310.

[6] A.A. Vasiljev, Shock Waves 3 (1994) 321-326.

[7] A.J. Higgins, A.P. Bruckner, AIAA paper (1996) 96-0342.

[8] J. Kasahara, T. Arai, S. Chiba, K. Takazawa, Y. Tanahashi, A. Matsuo, Proc. Combusti. Inst. 29 (2002) 2817-2824.

[9] M.J. Kaneshige, J.E. Shepherd, Proc. Combusti. Inst. 26 (1996) 3015-3022.

[10] J. Verreault, A.J. Higgins, Proc. Combusti. Inst. 33 (2011) 2311-2318.

[11] C. Li, K. Kailasanath, S. Oran, Phys. Fluids 6 (1994) 1600-1611.

[12] J.-Y. Choi, E.J.-R. Shin, I.-S.Jeung, Proc. Combusti. Inst.32 (2009) 2387-2396.

[13] J. Kasahara, T. Fujiwara, T. Endo, T. Arai, AIAA J. 39 (8) (2001) 1553-1561.

[14] S. Maeda, R. Inada, J. Kasahara, A. Matsuo, Proc. Combusti. Inst. 33 (2011) 2343-2349.

[15] S. Maeda, J. Kasahara, A. Matsuo, Combust. Flame 159 (2) (2012) 887-896.

[16] S. Maeda, J. Kasahara, A. Matsuo, The 28th ISTS Special Issue of Transactions of JSASS (2011), Accepted

in January 2012.

[17] M.J. Kaneshige, J.E. Shepherd, Detonation Database, Technical Report No. FM97-8, GALCIT, Pasadena, CA, 1997.

[18] W.C. Reynolds, The Element Potential Method for Chemical Equilibrium Analysis: Implementation in the Interactive Program STANJAN: Version 3, Technical Report No. A-3991, Stanford Univ., 1986.

[19] F.S. Billig, J. Spacecr. Rockets, 4 (1967) 822-823.

[20] L. He, P. Clavin, J. Fluid Mech. 277 (1994) 227-248.

[21] J. Yao, D.S. Stewart, Combust. Flame 100 (1995) 519-528.

[22] H. Nakayama, T. Moriya, J. Kasahara, A. Matsuo, Y. Sasamoto, I. Funaki, Combust. Flame 159 (2012) 859-869.

[23] J.H.S. Lee, The Detonation Phenomenon, Cambridge University Press, New York, 2008.

(437 words)

List of figure captions

Table 1. Experimental conditions.

Fig. 1. Continuous pictures of the initiation process of stabilized ODW (negative pictures).

Fig. 2. Schematic of the initiation process of stabilized ODW.

Fig. 3. Comparisons of the measured and calculated development rates of stabilized ODW.

Fig. 4. Superposed pictures of the stabilized ODW (6-μs intervals, negative pictures).

Fig. 5. Measured and fitted wave shapes of the stabilized ODW, and bow shock shapes which were measured and calculated from Billig's empirical correlation [19].

Fig. 6. Definitions of the curvature radiuses, and schematics of the velocity and curvature radius distributions.

Fig. 7. Schematic of the stabilizing criticality of detonation waves around the projectiles.

Fig. 8. Measured and fitted curvature radiuses and propagation velocities distributions for the $2C_2H_2+5O_2+21Ar$ mixture.

Fig. 9. Critical curvature radiuses of the curved detonation waves.

Table 1. Experimental conditions.

No.	Mixture	V_p / D_{CJ}	d / λ
-	-	±1 %	±0.5 %
Initiation process w/ diaphragm rapture			
1-1	$2C_2H_2+5O_2+7Ar$	1.18	4.3
1-2		1.07	5.0
Initiation process w/o diaphragm rapture			
1-3	$2C_2H_2+5O_2+7Ar$	1.14	3.6
1-4		1.31	3.6
1-5		1.08	4.2
1-6		1.22	4.0
1-7		1.09	4.9
1-8		1.25	4.8
1-9		1.06	6.3
1-10		1.22	6.1
Well downstream of the initiation process			
2-1	$2C_2H_2+5O_2+7Ar$	1.25	4.1
2-2		1.20	4.9
2-3		1.07	7.6
2-4	$2C_2H_2+5O_2+21Ar$	1.29	5.8
2-5		1.31	6.5
2-6		1.31	8.0
2-7	$C_2H_4+3O_2+4Ar$	1.09	3.8
2-8		1.22	4.1
2-9		1.23	4.6
2-10	$2H_2+O_2+3Ar$	1.26	3.8
2-11		1.21	4.2
2-12		1.23	4.7

(228 words)

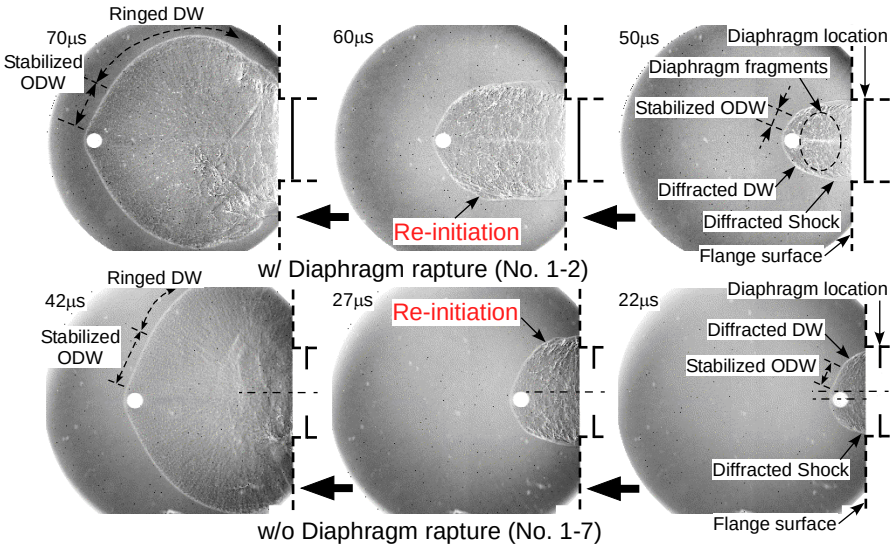

Fig. 1. Continuous pictures of the initiation process of stabilized ODW (negative pictures).

(363 words)

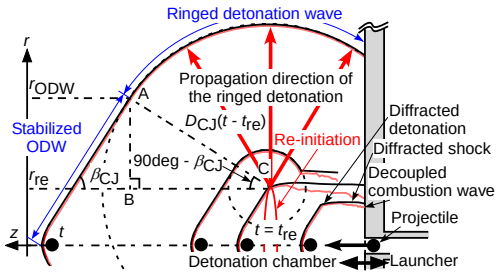

Fig. 2. Schematic of the initiation process of stabilized ODW.

(112 words)

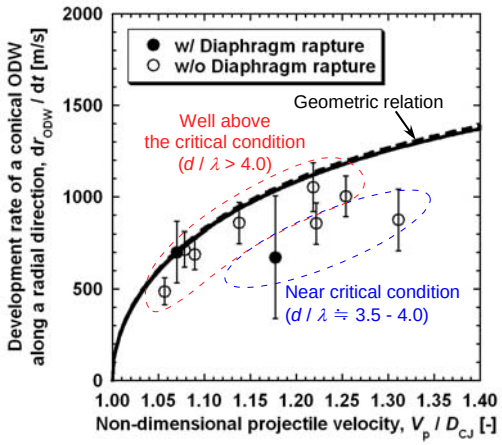

Fig. 3. Comparisons of the measured and calculated development rates of stabilized ODW.

(167 words)

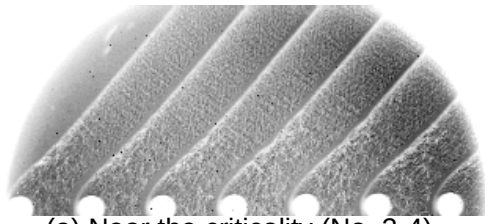

(a) Near the criticality (No. 2-4)

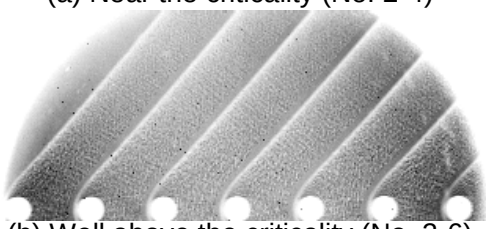

(b) Well above the criticality (No. 2-6)

Fig. 4. Superposed pictures of the stabilized ODW (6-μs intervals, negative pictures).

(170 words)

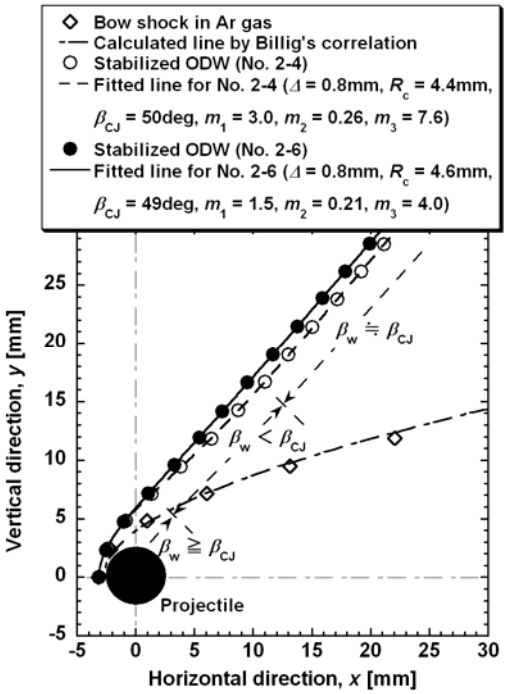

Fig. 5 Measured and fitted wave shapes of the stabilized ODW, and bow shock shapes which were measured and calculated from Billig's empirical correlation [19].

(250 words)

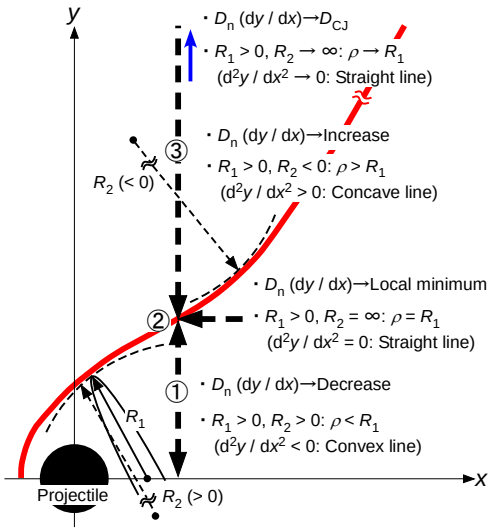

Fig. 6. Definitions of the curvature radiuses, and schematics of the velocity and curvature radius distributions.

(192 words)

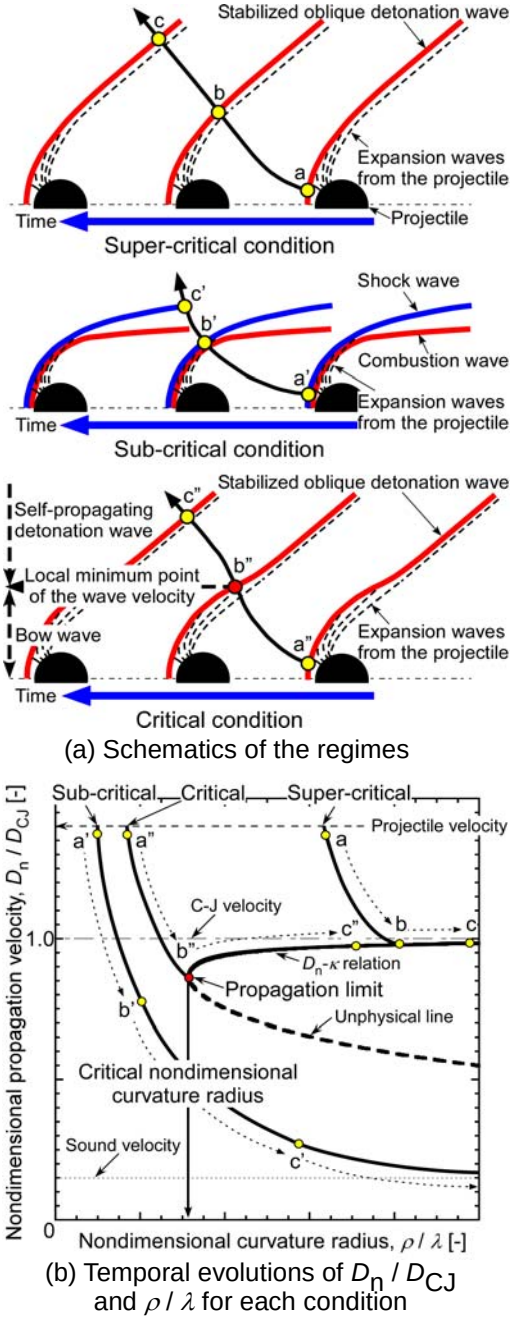

Fig. 7. Schematic of the stabilizing criticality of detonation waves around the projectiles.

(418 words)

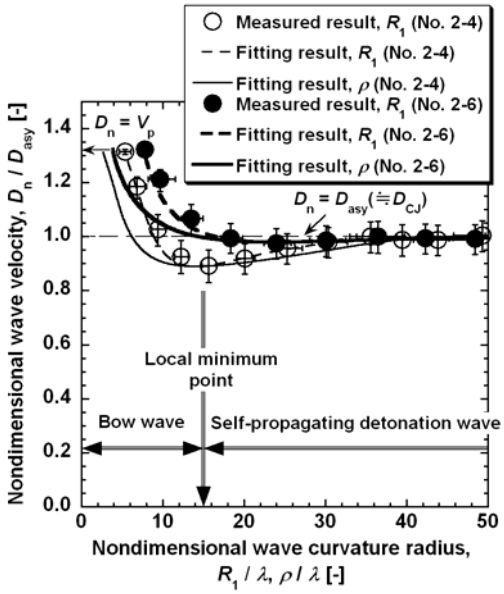

Fig. 8. Measured and fitted curvature radiuses and propagation velocities distributions for the $2C_2H_2+5O_2+21Ar$ mixture.

(213 words)

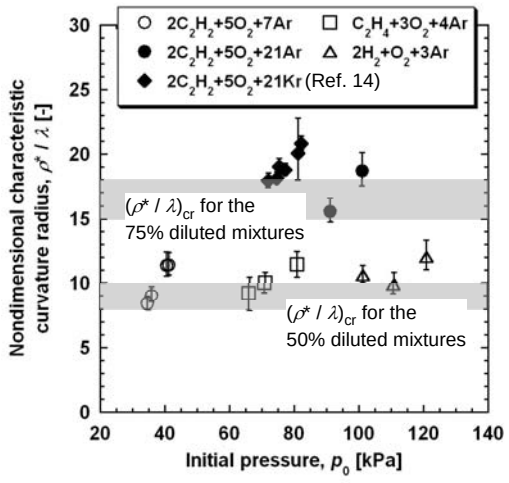

Fig. 9. Critical curvature radiuses of the curved detonation waves.

(173 words)